PLANT SCIENCE

Cell polarity linked to gravity sensing is generated by LZY translocation from statoliths to the plasma membrane

Takeshi Nishimura[1,2]†, Shogo Mori[1]†, Hiromasa Shikata[1,2]†, Moritaka Nakamura[1], Yasuko Hashiguchi[3]‡, Yoshinori Abe[4], Takuma Hagihara[4], Hiroshi Y. Yoshikawa[5], Masatsugu Toyota[4,6,7], Takumi Higaki[8,9], Miyo Terao Morita[1,2]*

Organisms have evolved under gravitational force, and many sense the direction of gravity by means of statoliths in specialized cells. In flowering plants, starch-accumulating plastids, known as amyloplasts, act as statoliths to facilitate downstream gravitropism. The gravity-sensing mechanism has long been considered a mechanosensing process by which amyloplasts transmit forces to intracellular structures, but the molecular mechanism underlying this has not been elucidated. We show here that LAZY1-LIKE (LZY) family proteins involved in statocyte gravity signaling associate with amyloplasts and the proximal plasma membrane. This results in polar localization according to the direction of gravity. We propose a gravity-sensing mechanism by which LZY translocation to the plasma membrane signals the direction of gravity by transmitting information on the position of amyloplasts.

Plants sense their inclination relative to the direction of gravity and reorient their growth direction accordingly, a process called gravitropism (*1*, *2*). The directional change is sensed mainly by specialized cells called statocytes. Statocytes contain amyloplasts, which are plastids filled with dense starch granules (*3*, *4*). Amyloplasts act as statoliths within cells by displacing toward gravity. Amyloplast displacement is believed to promote auxin transport in the direction of gravity, leading to organ bending (*5*). Several hypotheses have been proposed regarding the sensing mechanism by which the physical process of amyloplast displacement generates biochemical signals in statocytes, including the force-sensing model (*6*) and position sensor hypothesis (*7*). However, the molecular mechanisms of gravity sensing and signaling remain largely unknown.

LAZY1-LIKE (*LZY*) family genes, which are conserved in most land plants, are involved in gravitropism and whole-plant architecture through the control of branch angles in various species in angiosperms, including trees (*8*–*15*). In *Arabidopsis*, LZY proteins have been shown to play critical roles in the signaling process controlling directional auxin flow after amyloplast displacement in statocytes in both shoots and roots (*16*). Although there are no known functional domains in LZY proteins, five conserved regions with 10 to 20 amino acids were found (fig. S1A) (*2*, *10*). Mutational analyses have demonstrated the functional importance of regions I, II (also known as IGT motif) (*15*, *17*), and V (CCL region) (*16*, *18*). LZY1, rice LAZY1, and maize ZmLA1 localize to the plasma membrane (PM) and the nucleus in ectopic or transient expression systems. As a result, possible functions in the nucleus in addition to the PM have been suggested (*14*, *19*, *20*). It should be noted that, under the control of its own promoter, LZY3 is polarly localized to the PM in the direction of gravity and repolarizes in response to the reorientation in statocytes in the columella cells of lateral roots (*21*). This finding prompted us to investigate the mechanism of LZY3 polarization to understand gravity sensing and signaling in gravitropism.

Regions for functional regulation of LZY3

We determined the regions responsible for membrane association in the LZY3 protein, which lacked detectable transmembrane domains (by InterProScan) (*22*). Basic-hydrophobic clusters in proteins can facilitate their membrane association in eukaryotes, including plants (*23*–*25*). A computational search indicated that all LZY proteins in *Arabidopsis* have more than two regions with a high basic-hydrophobic cluster score (≥0.6) that have the potential to serve as unstructured membrane-binding sites (fig. S1, A and B) (*23*). Glutamine (Gln) substitutions were introduced at two sites, designated sites A and B, in LZY3 that decreased the basic-hydrophobic cluster scores of the corresponding sites (Fig. 1A and fig. S1B). Whereas the primary roots of *lzy2;3;4* triple mutants tended to grow upward (*2*), the expression of LZY3 fused with mCherry (LZY3-mCherry) harboring A-7Q, A-10Q, and B-7Q substitutions, as well as wild type (WT), rescued the primary root angle phenotypes of *lzy2;3;4* under the control of the LZY3 promoter (Fig. 1B and fig. S1, D and E). Plants expressing LZY3 B-11Q exhibited variable growth directions (Fig. 1B and fig. S1D). The LZY3-mCherry signals of WT, A-7Q, and B-7Q were faint in the living columella cells of the primary roots. In contrast, the signals of A-10Q and B-11Q exhibited observably increased fluorescence to different extents (Fig. 1C and fig. S1, C and G). The fluorescence signals of A-10Q accumulated at the lower side of the PM, whereas the signals of B-11Q were mainly detected in the cytosol (Fig. 1, C and D). Combination of B-7Q with A-7Q or A-10Q increased the LZY3-mCherry levels and the relative fluorescence intensities in the cytosol, which is consistent with their lower degree of phenotypic rescue in gravitropism (Fig. 1, C and D, and fig. S1, C, F, and G). LZY3-mCherry that has both A-10Q and B-11Q was mostly found in the cytosol, as was the version with only B-11Q (Fig. 1C). These findings suggest that sites B and A, including their surrounding sequences, play major and minor roles, respectively, in PM association of LZY3, possibly through electrostatic interactions with anionic membrane lipids, and that both regions help maintain LZY3 at low levels (fig. S1G).

A putative PEST motif (i.e., a motif enriched with Pro, Glu, Ser, and Thr), which may facilitate protein degradation via the proteasome pathway, is found in the vicinity of site A, implying that it may be involved in the regulation of LZY3 levels (fig. S2A) (*26*, *27*). The predicted PEST score of A-10Q is reduced compared with wild-type LZY3, whereas that in A-7Q is not affected (fig. S2A). As expected, LZY3ΔPEST-mCherry, which lacks the PEST motif without impairing site A itself, displayed similarities to A-10Q in terms of root growth angle, localization pattern within columella cells, and accumulation level within those cells (fig. S2, B to D). These findings suggest that the accumulation of LZY3-mCherry on the PM in A-10Q lines resulted from impairment of the PEST motif, thereby disturbing quantitative regulation of LZY3 on the PM through proteasomal protein degradation. The addition of a farnesylation site [K8-far (*28*)] at the C termini of LZY3 mutant proteins B-11Q and A-10Q;B-11Q overrode the effect of their mutation on localization and activity (fig. S3). These results suggest that the B-11Q and A-10Q;B-11Q proteins retain all functions of the wild-type LZY3 with the exception of association with the PM. In addition, when K8-far was present, the level of the B-11Q protein was reduced, implying a link between the membrane localization and quantitative regulation

[1]Division of Plant Environmental Responses, National Institute for Basic Biology, Okazaki 444-8585, Japan. [2]Course for Basic Biology, The Graduate Institute for Advanced Studies, SOKENDAI, Hayama 240-0115, Japan. [3]Graduate School of Bioagricultural Sciences, Nagoya University, Nagoya 464-8601, Japan. [4]Department of Biochemistry and Molecular Biology, Saitama University, Saitama 338-8570, Japan. [5]Department of Applied Physics, Osaka University, Suita 565-0871, Japan. [6]Suntory Rising Stars Encouragement Program in Life Sciences (SunRiSE), Suntory Foundation for Life Sciences, Kyoto 619-0284, Japan. [7]Department of Botany, University of Wisconsin, Madison, WI 53706, USA. [8]Faculty of Advanced Science and Technology, Kumamoto University, Kumamoto 860-8555, Japan. [9]International Research Organization for Advanced Science and Technology, Kumamoto University, Kumamoto 860-8555, Japan.
*Corresponding author. Email: mimorita@nibb.ac.jp
†These authors contributed equally to this work.
‡Present address: JOCAVIO Co. Ltd., Fukuoka 839-0864, Japan.

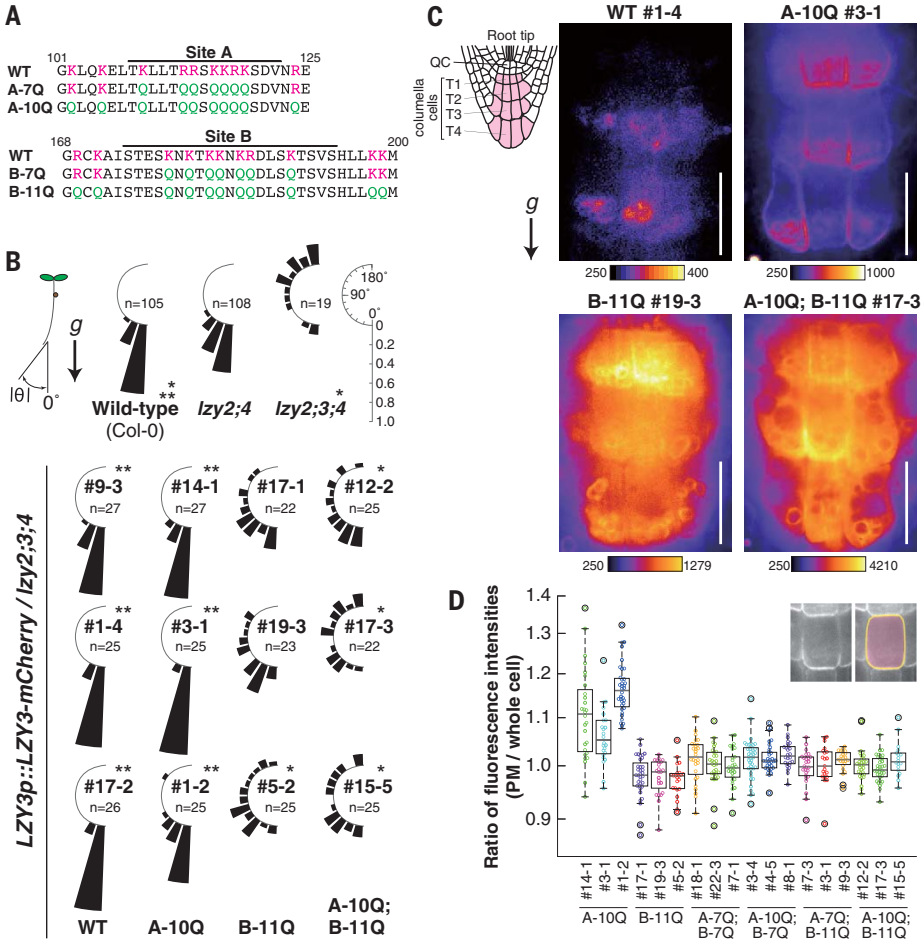

Fig. 1. A putative membrane association site in LZY3 is required for subcellular localization in the columella cells and for root gravitropism. (**A**) Putative PM association sites in LZY3. The lines indicate sites with basic-hydrophobic scores ≥ 0.6 according to computational prediction. In A-7Q and A-10Q, 7 and 10 basic amino acid residues at and near site A, respectively, were replaced with glutamine residues. In B-7Q and B-11Q, 7 and 11 basic residues at and nearby site B, respectively, were replaced with glutamine residues. The basic residues (K and R) and glutamine residue (Q) are colored magenta and green, respectively. Single-letter abbreviations for the amino acid residues are as follows: A, Ala; C, Cys; D, Asp; E, Glu; F, Phe; G, Gly; H, His; I, Ile; K, Lys; L, Leu; M, Met; N, Asn; P, Pro; Q, Gln; R, Arg; S, Ser; T, Thr; V, Val; W, Trp; and Y, Tyr. (**B**) Absolute values of growth angle (θ) of the primary root tips of 5-day-old seedlings of wild-type, *lzy2;4*, *lzy2;3;4*, and transgenic lines expressing mCherry-tagged LZY3 mutant proteins under the control of the *LZY3* promoter (*LZY3p::LZY3-mCherry*) in the *lzy2;3;4* mutant background. The direction of each root tip was measured as the absolute value toward the direction of gravity (*g*). The frequency was calculated as the proportion of root numbers that fell within intervals of 15° to the total number of analyzed roots for each line (range: 0° to 180°). Asterisks indicate significant differences [$P < 0.0033$ (0.05/15)] by Wilcoxon rank sum test with Bonferroni correction (*, compared with *lzy2;4*; **, compared with *lzy2;3;4*). (**C**) Representative confocal images of wild-type, A-10Q, B-11Q, and A-10Q;B-11Q mutants of LZY3-mCherry in columella cells of primary roots. The area containing tier 1 to 3 columella cells of the representative lines is shown. The seedlings were kept in a vertical position before and during imaging. The roots of the B-11Q and A-10Q;B-11Q lines were straightened at least 3 hours before imaging to make the amyloplasts sediment toward the root tip, as those roots were meandering (fig. S1D). All images were acquired with an identical optical setting, and the color-coded heatmaps for signal intensities appear below each image. Scale bars, 20 μm. QC, quiescent center. (**D**) Ratio of fluorescence intensities of LZY3-mCherry at the PM to that of the whole cell. The ratios were calculated with mean values within a 3-pixel-width line drawn on the PM region and within the area surrounded by the line. For each line, 19 to 41 cells with clear cell edges in 5 to 8 roots were measured. Wild-type, A-7Q, and B-7Q lines were not analyzed because of low protein accumulation.

of LZY3. Taken together, these findings indicate that the PM localization of LZY3 is required for its function in gravity signaling.

LZYs associate with amyloplasts and the nearby PM

Meanwhile, we noticed faint ring-shaped fluorescence signals in the tier 3 columella cells of wild-type LZY3-mCherry, which were observed at the position of amyloplasts (Fig. 1C). Given that LZY localizes to amyloplasts, LZY might help link gravity sensing to the downstream signaling. However, the weak fluorescence intensity of LZY3-mCherry made it difficult to analyze the behavior of LZY3 in tier 2 cells, which are the major contributors to gravitropism (*29*). Therefore, we examined whether LZY4, which redundantly functions in root gravitropism (*30*, *31*), can be applied for live-cell imaging analysis. There are four splicing variants of LZY4 (annotated in the TAIR10 genome), three of which lack the CCL region (fig. S4, A and B), which is important for LZY1/2/3 function (*16*, *18*, *21*). We demonstrated that LZY4.4 with a CCL-like sequence is the functional form in gravitropism (fig. S4C). The CCL-like sequence of LZY4.4 was capable of interacting with the BREVIS RADIX (BRX) domain of RCC1-like domain proteins (RLDs) in the yeast two-hybrid system (fig. S4D). RLD1 is an interacting partner of LZY in the regulation of auxin transport through membrane trafficking, and it is recruited to the PM in a LZY2/3-dependent manner (*21*, *32*). LZY4.4 recruited RLD1 to the PM in *Arabidopsis* protoplasts (fig. S5). In addition, *LZY4.4-mClover3* driven by the statocyte-specific *ADF9* promoter rescued the primary root angle phenotype of *lzy1;2;3;4* (fig. S6). These results indicate that the molecular function of LZY4.4 (hereafter referred to as LZY4) is almost equivalent to that of LZY3 in root statocytes.

Ring-shaped and linear fluorescence signals from functional *LZY4p::LZY4-mScarlet* were observed in the tier 2 columella cells of both young lateral and primary roots (Fig. 2, A and B, and fig. S7A). The linear fluorescence signal merged with that from the PM-staining reagent (fig. S8), which confirms the PM localization of LZY4. LZY4-mScarlet on the PM was observed only proximal to amyloplasts, implying polarity in the direction of gravity (Fig. 2A). LZY4 also has a basic amino acid–rich region in the middle of the protein (basic-hydrophobic cluster score ≥ 0.6; figs. S1A and S9A). LZY4-mScarlet carrying the B-6Q mutation in this region exhibited lower fluorescence at the PM, lack of polarity, and weaker capacity for phenotypic rescue, suggesting a PM-binding mechanism and function similar to LZY3 (Fig. 2, B and C, and figs. S7B and S9B). To investigate the association of the ring-shaped signal of LZY4-mScarlet with amyloplasts, we conducted observations using green fluorescent protein–fused PERMEASE IN CHLOROPLASTS1

(PIC1-GFP) and OUTER ENVELOPE MEMBRANE PROTEIN 7 (OEP7-GFP), both of which serve as plastid markers localized at an inner and outer envelope of plastids, respectively. These observations were performed on both living and fixed lateral root columella cells. LZY4-mScarlet was observed in close proximity to or partially overlapping with PIC1-GFP and OEP7-GFP, indicating that LZY4 likely localizes to the amyloplast envelopes or their immediate vicinity (Fig. 2D and fig. S10). However, defining the exact localization of LZY4 in amyloplasts remains challenging because of the weak expression levels of LZY4-mScarlet and the envelope markers, as well as technical limitations.

Next, we generated LZY4-mScarlet lacking the N-terminal domain I (LZY4-ΔI-mScarlet) and found that the protein was present at the PM and in the cytosol, but the ring-shaped signal was hardly detected (Fig. 2E and fig. S7C). In addition, LZY4-ΔI-mScarlet was not fully functional (Fig. 2B). Consistently, mCherry fused with the N-terminal 54 amino acids of LZY3, including the conserved domain I, displayed obvious ring-shaped signals (fig. S11). These findings suggest that the N-terminal region including domain I is involved in the amyloplast localization of LZY3/4.

Several mutations in genes encoding components of the translocon at the outer chloroplast membrane (TOC) complex enhance the phenotype of *altered response to gravity 1* (*arg1*) and its paralog *arg1-like2* (*arl2*) (*33*, *34*). *ARG1* and *ARL2*, encoding J-domain proteins, are involved in gravity signaling in statocytes (*35*–*37*) similarly to *LZYs*. We investigated the possible involvement of ARG1 and ARL2 in the amyloplast localization of LZY4-mScarlet. In the *arg1* and *arl2* background, the LZY4-mScarlet signal became undetectable in amyloplasts and at the PM, and the signal was dispersed in the cytosol (Fig. 2F and figs. S7, D and E, and S12). ARG1 and ARL2 may be involved in the recruitment of LZYs to amyloplasts, possibly through their chaperone activity. We cannot rule out the possibility that ARG1 and ARL2 might also be involved in the PM localization of LZYs, because ARL2 is reported to localize at the PM (*36*). Considering that precursor proteins targeted to plastids interact with TOC through their N-terminal transit peptides with the help of molecular chaperones (*38*), mechanisms similar to plastid protein targeting could be involved in targeting LZYs to amyloplasts. Further investigations into the precise localization of LZYs in amyloplasts and their targeting mechanisms are warranted to gain a deeper understanding of the LZY-mediated interaction between the amyloplast and PM.

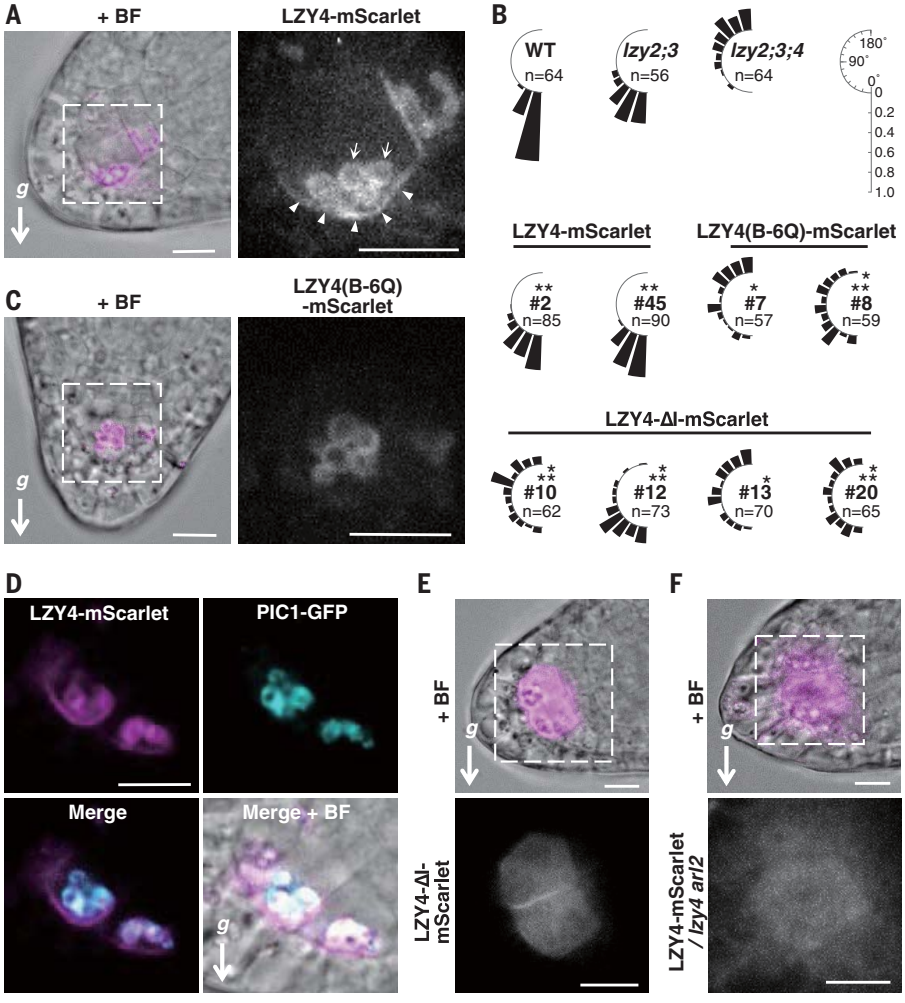

Fig. 2. Amyloplast and basal plasma membrane localization of LZY4 in the columella cells. (**A**) Subcellular localization of LZY4-mScarlet (#2)/*lzy4* in lateral root columella cells. Arrows in the right panel indicate the amyloplast-like ring shape localization of LZY4-mScarlet, and arrowheads indicate the localization to the basal plasma membrane. BF, bright field. Scale bars, 10 μm. (**B**) Complementation test of *LZY4-mScarlet/lzy2;3;4*, *LZY4(B-6Q)-mScarlet/lzy2;3;4*, and *LZY4-ΔI-mScarlet/lzy2;3;4* in the direction of the primary root tips of 5-day-old seedlings. Asterisks indicate significant differences [$P < 0.0045$ (0.05/11)] by Wilcoxon rank sum test with Bonferroni correction (*, compared with *lzy2;3*; **, compared with *lzy2;3;4*). (**C**) Subcellular localization of LZY4(B-6Q)-mScarlet (#7)/*lzy2;3;4* in lateral root columella cells. Scale bars, 10 μm. (**D**) Localization of LZY4-mScarlet and PIC1-GFP in amyloplasts. Scale bar, 10 μm. (**E**) Subcellular localization of LZY4-ΔI-mScarlet (#12)/*lzy2;3;4*. Scale bars, 10 μm. (**F**) Subcellular localization of LZY4-mScarlet (#2) in the *lzy4 arl2* mutant background. Scale bars, 10 μm.

LZY4 polarity rapidly changes upon gravistimulation

Next, we examined the effect of gravistimulation by reorientation of plants on the localization of LZY4-mScarlet. We used live-cell imaging of lateral root columella cells with a vertical stage confocal microscope (*39*). Before gravistimulation, polar localization of LZY4-mScarlet on the PM was maintained throughout the observation, although amyloplasts were slightly agitated (fig. S13B and movie S1). After gravistimulation, LZY4-mScarlet appeared on the PM of the new lower side of the cells at almost the same time as amyloplast displacement, and the signal gradually became stronger (Fig. 3, A and B; fig. S13C; and movie S2). Simultaneously, the LZY4-mScarlet signal on the PM in the original direction of gravity gradually disappeared, resulting in the generation of the new polarity of LZY4. Such repolarization on the PM was not observed with LZY4(B-6Q)-mScarlet (fig. S14 and movie S3). The starchless *phosphoglucomutase* (*pgm*) mutant has amyloplasts that hardly sediment, because of the lack of dense starch granules, and it exhibits reduced gravitropism (*40*–*42*). In the *pgm* mutant, LZY4-mScarlet localized to smaller starchless amyloplasts and to the PM. LZY4-mScarlet failed to accumulate polarly on the PM in the *pgm* mutant, probably because of altered movement of amyloplasts (Fig. 3C,

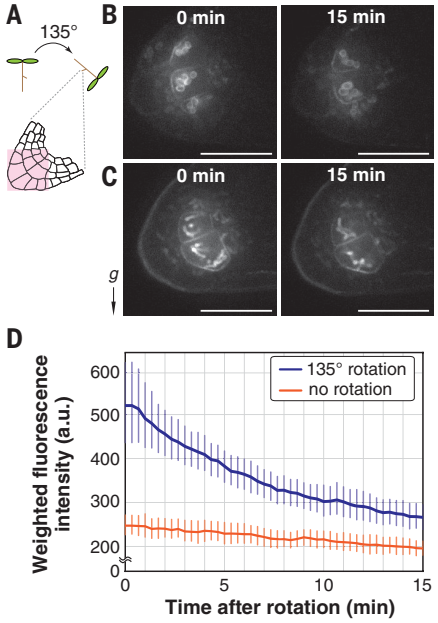

Fig. 3. Polar localization of LZY4 changes in response to gravistimulation. (**A**) Gravistimulation and the site of observation. Stage 2 lateral roots (<3 mm) were used. (**B** and **C**) Representative confocal images of the columella cells of *LZY4p::LZY4-mScarlet* in the *lzy4* (B) or *lzy4 pgm-1* (C) background immediately before (0 min) or 15 min after gravistimulation. The seedlings were kept in a vertical position before and during imaging. mScarlet was excited at 561 nm, and the fluorescence that passed through a 617/73 nm emission filter was detected. Scale bars, 25 μm. (**D**) Temporal changes in the localization of LZY4-mScarlet on the PM along the direction of gravity. Images were taken at 20-s intervals for 15 min. Eight cells from five of the nonrotated lateral roots and 17 cells from 11 of the 135°-rotated lateral roots were used for quantification. Error bars indicate 95% confidence intervals. a.u., arbitrary units.

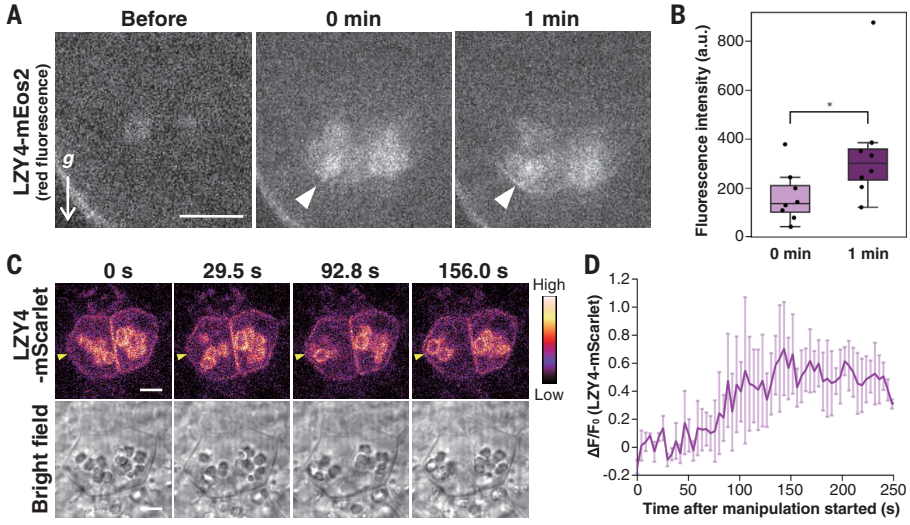

Fig. 4. Translocation of LZY4 from the amyloplast to the plasma membrane. (**A** and **B**) Observation of the translocation of LZY4-mEos2 from the amyloplasts to the PM by the photoconversion method (A). Immediately after photoconversion, there was almost no red fluorescence signal on the PM (white arrowhead at 0 min). At 1 min after photoconversion, a linear red fluorescence signal was observed at the PM in close proximity to the amyloplasts (white arrowhead at 1 min). Scale bar, 10 μm. There was a significant difference between the findings at 0 and 1 min (Wilcoxon rank sum test, $P < 0.05$). The increase in the red fluorescence signal on the PM at 1 min after photoconversion was quantitatively analyzed and plotted as boxplots. Center lines show the medians; box limits indicate the 25th and 75th; whiskers extend 1.5 times the interquartile range from the 25th and 75th percentiles; outliers are represented by dots (B). The plots represent the results of eight independent experiments. See also fig. S21B, showing images of mEos2 green fluorescence signals. (**C** and **D**) Temporal changes in the localization of LZY4-mScarlet upon manipulating amyloplasts with an optical tweezer. Amyloplasts were fixed with the optical tweezer and positioned near the PM (yellow arrowheads) by moving the roots immobilized on the stage. The representative change is shown in (C). Scale bar, 5 μm. The temporal changes in the signal of mScarlet on the PM where the amyloplasts were positioned are quantitatively shown in (D). The plot represents the mean ± standard error of three independent experiments.

fig. S15, and movie S4), indicating that amyloplast sedimentation is required for the polarization of LZY4 on the PM.

We quantified the temporal change in the localization of the LZY4-mScarlet signal at the PM along the direction of gravity (Fig. 3D and fig. S16). Briefly, to focus on the change in the fluorescence intensities on the PM along the vertical line (*y* axis), the intensities on the PM were averaged along the *x* axis (fig. S16, A to H). Then, each averaged value along the *y* axis was multiplied by a value (between 1 and 100) assigned to the same position on the *y* axis, which is linearly distributed from the bottom to the top of the intensity profile (fig. S16, I and J). The calculated values were integrated for each time frame (fig. S16K), and this weighting process was designed to produce progressively lower integrated values over time as LZY4-mScarlet moves toward the direction of gravity. Thus, a higher value of weighted intensity means that LZY4-mScarlet polarizes at a higher position on the PM, whereas a lower value means that LZY4-mScarlet polarizes in the direction of gravity. Without gravistimulation, the weighted intensity gradually and slightly decreased, probably because of quenching during the 15-min observation. In contrast, weighted intensity decreased after gravistimulation, indicating repolarization of LZY4-mScarlet in the direction of gravity. An incremental decrease in weighted intensity occurred immediately after gravistimulation, presumably linked with amyloplast displacement.

To clarify the temporal relationship between the repolarization of LZY4 and other processes in gravitropism, we examined LZY4-mScarlet repolarization, auxin distribution, and organ curvature with primary roots under as similar conditions as possible (fig. S17). The behavior of LZY4-mScarlet in primary roots was almost the same as that in lateral roots. Significant repolarization of LZY4-mScarlet was detected within 15 min after gravistimulation (fig. S17, A to C, and movie S5). The asymmetric distribution of auxin, detected using the ratiometric auxin biosensor R2D2 (*43*), appeared 16 min after gravistimulation, and it became significant at 30 min (fig. S17, D and E). Significant root curvature appeared 30 min after gravistimulation (fig. S17F). In addition, amyloplast displacement occurred 3 min after gravistimulation in our observation system, as previously reported (*16*). Polar localization of RLD1-GFP merged with LZY4-mScarlet was observed at 15 min after gravistimulation (fig. S18). Therefore, repolarization of LZY4-mScarlet is chronologically consistent with a role in linking gravity sensing to signaling. Although we tested relocation of PIN3-GFP upon gravistimulation according to the measurement method reported previously (*21*, *44*), obvious relocation was not detected within 15 min (fig. S19). As reported previously, the polar pattern of PIN3-GFP in the root cap columella after gravistimulation was observed 300 min after gravistimulation in the stage 2 lateral root in our experimental conditions (*21*). This implies that the LZY-RLD module may not directly regulate the trafficking of PIN3 but rather regulates other regulatory factors for auxin transport.

Amyloplast position determines LZY4 polarity at the PM

Given that LZY interacts electrostatically with negatively charged lipids, such lipids might polarly distribute on the PM and contribute to the polar localization of LZYs. Therefore, we examined the distribution of several negatively charged lipids in the statocytes of primary

and lateral roots using fluorescent biosensors (fig. S20). Only the phosphatidylinositol-4,5-bisphosphate biosensor CITRINE-2xPH^{PLC} (*45*) tended to be polarly distributed toward the root tip. However, clear repolarization of CITRINE-2xPH^{PLC} was not detected upon gravistimulation in the examined time window. Therefore, the distribution of these lipids is unlikely to be related to the polarity of LZYs.

Next, to elucidate the relationship between LZY4 residing in amyloplasts and its polarization at the PM, the behavior of LZY4 was analyzed using the *LZY4p::LZY4-mEos2/lzy1;2;3;4* rescued line (fig. S21A). LZY4-mEos2 on the amyloplasts was photoconverted from green to red fluorescence by irradiation with a 405-nm laser on a vertical stage confocal microscope. The red fluorescence signal was observed only in amyloplasts immediately after irradiation, and a linear pattern emerged on the nearby PMs (Fig. 4A; figs. S21, B and C, and S22; and movie S6). The fluorescence intensity on the PM proximal to amyloplasts significantly increased 1 min after irradiation (Fig. 4B). Although we could not dismiss the possibility that a trace amount of cytoplasmic LZY4-mEos2 was photoconverted and accumulated at the PM, this result suggests that LZY4 is rapidly translocated from amyloplasts to the PM. It is expected that the position of amyloplasts determines the LZY4 accumulation site on the PM independent of the direction of gravity. To test this possibility, amyloplasts were manipulated by an optical tweezer during observation by confocal laser scanning microscopy (*46*). After trapping some amyloplasts, the amyloplasts were manipulated into close proximity of the PM (figs. S23 and S24 and movies S7 and S8). The fluorescence intensity of LZY4-mScarlet significantly increased at the PM region where the amyloplasts were newly placed nearby (Fig. 4, C and D; fig. S23, G to L; and movie S9), indicating that amyloplasts act as determinants of LZY4 polarity on the PM.

Gravity sensing in gravitropism has long been considered a mechanosensing mechanism whereby the weight of statoliths exerts a force on intracellular structures (*6*, *47*). On the basis of the experimental results using angiosperm shoots, it has recently been suggested that the sensor functions as a clinometer but not as a force sensor (*48*). This supports the "position sensor hypothesis," which proposes that proximity or contact between statoliths and the membrane induces local auxin fluxes (*7*) and that statocytes act as clinometers (*49*), although there had been no known molecules supporting this hypothesis. We revealed in this study that LZY exhibits behavior that fits the position sensor hypothesis well. LZY polarity on the PM formed according to the position of amyloplasts by translocation of LZY from amyloplasts to the PM (fig. S25A). LZY appears to act as a signal molecule that transmits the positional information of statoliths to the PM, which directly links gravity sensing to subsequent signaling processes. Polarly located LZY recruits RLD to promote polar auxin flow in the direction of gravity (fig. S25B) (*21*).

REFERENCES AND NOTES

1. S.-H. Su, P. H. Masson, in *Sensory Biology of Plants*, S. Sopory, Ed. (Springer, 2019), pp. 95–136.
2. N. Kawamoto, M. T. Morita, *New Phytol.* **236**, 1637–1654 (2022).
3. F. D. Sack, *Planta* **203** (suppl. 1), S63–S68 (1997).
4. M. T. Morita, *Annu. Rev. Plant Biol.* **61**, 705–720 (2010).
5. H. Han, M. Adamowski, L. Qi, S. S. Alotaibi, J. Friml, *New Phytol.* **232**, 510–522 (2021).
6. G. Perbal, D. Driss-Ecole, *Trends Plant Sci.* **8**, 498–504 (2003).
7. O. Pouliquen *et al*., *Phys. Biol.* **14**, 035005 (2017).
8. P. Li *et al*., *Cell Res.* **17**, 402–410 (2007).
9. T. Yoshihara, M. Iino, *Plant Cell Physiol.* **48**, 678–688 (2007).
10. T. Yoshihara, E. P. Spalding, M. Iino, *Plant J.* **74**, 267–279 (2013).
11. Z. Dong *et al*., *Plant Physiol.* **163**, 1306–1322 (2013).
12. Y. Uga *et al*., *Nat. Genet.* **45**, 1097–1102 (2013).
13. J. Salojärvi *et al*., *Nat. Genet.* **49**, 904–912 (2017).
14. A. Ashraf *et al*., *PLOS ONE* **14**, e0214145 (2019).
15. J. M. Waite, C. Dardick, *Curr. Opin. Plant Biol.* **59**, 101983 (2021).
16. M. Taniguchi *et al*., *Plant Cell* **29**, 1984–1999 (2017).
17. J. M. Guseman, K. Webb, C. Srinivasan, C. Dardick, *Plant J.* **89**, 1093–1105 (2017).
18. T. Yoshihara, E. P. Spalding, *Plant Physiol.* **182**, 1039–1051 (2020).
19. Z. Li *et al*., *Mol. Plant* **12**, 1143–1156 (2019).
20. T. P. Howard III *et al*., *PLOS ONE* **9**, e87053 (2014).
21. M. Furutani *et al*., *Nat. Commun.* **11**, 76 (2020).
22. T. Paysan-Lafosse *et al*., *Nucleic Acids Res.* **51**, D418–D427 (2023).
23. H. Brzeska, J. Guag, K. Remmert, S. Chacko, E. D. Korn, *J. Biol. Chem.* **285**, 5738–5747 (2010).
24. M. L. A. Simon *et al*., *Nat. Plants* **2**, 16089 (2016).
25. I. C. Barbosa *et al*., *Development* **143**, 4687–4700 (2016).
26. S. Rogers, R. Wells, M. Rechsteiner, *Science* **234**, 364–368 (1986).
27. M. L. Spencer, M. Theodosiou, D. J. Noonan, *J. Biol. Chem.* **279**, 37069–37078 (2004).
28. S. Clarke, *Annu. Rev. Biochem.* **61**, 355–386 (1992).
29. E. B. Blancaflor, J. M. Fasano, S. Gilroy, *Plant Physiol.* **116**, 213–222 (1998).
30. L. Ge, R. Chen, *Nat. Plants* **2**, 16155 (2016).
31. T. Yoshihara, E. P. Spalding, *Plant Physiol.* **175**, 959–969 (2017).
32. L. Wang *et al*., *Nat. Commun.* **13**, 7 (2022).
33. J. P. Stanga, K. Boonsirichai, J. C. Sedbrook, M. S. Otegui, P. H. Masson, *Plant Physiol.* **149**, 1896–1905 (2009).
34. A. K. Strohm, G. A. Barrett-Wilt, P. H. Masson, *Front. Plant Sci.* **5**, 148 (2014).
35. J. C. Sedbrook, R. Chen, P. H. Masson, *Proc. Natl. Acad. Sci. U.S.A.* **96**, 1140–1145 (1999).
36. K. Boonsirichai, J. C. Sedbrook, R. Chen, S. Gilroy, P. H. Masson, *Plant Cell* **15**, 2612–2625 (2003).
37. B. R. Harrison, P. H. Masson, *Plant J.* **53**, 380–392 (2008).
38. P. Chotewutmontri, K. Holbrook, B. D. Bruce, *Int. Rev. Cell Mol. Biol.* **330**, 227–294 (2017).
39. M. Nakamura, M. Toyota, M. Tasaka, M. T. Morita, *Methods Mol. Biol.* **1309**, 57–69 (2015).
40. J. Z. Kiss, R. Hertel, F. D. Sack, *Planta* **177**, 198–206 (1989).
41. T. Caspar, B. G. Pickard, *Planta* **177**, 185–197 (1989).
42. N. Saether, T.-H. Iversen, *Planta* **184**, 491–497 (1991).
43. C.-Y. Liao *et al*., *Nat. Methods* **12**, 207–210, 2, 210 (2015).
44. P. Grones *et al*., *Sci. Rep.* **8**, 10279 (2018).
45. M. L. A. Simon *et al*., *Plant J.* **77**, 322–337 (2014).
46. Y. Abe *et al*., *Plant Biotechnol. (Tokyo)* **37**, 405–415 (2020).
47. G. Leitz, B.-H. Kang, M. E. A. Schoenwaelder, L. A. Staehelin, *Plant Cell* **21**, 843–860 (2009).
48. H. Chauvet, O. Pouliquen, Y. Forterre, V. Legué, B. Moulia, *Sci. Rep.* **6**, 35431 (2016).
49. A. Bérut *et al*., *Proc. Natl. Acad. Sci. U.S.A.* **115**, 5123–5128 (2018).

ACKNOWLEDGMENTS

We are grateful to N. Kawamoto (National Institute for Basic Biology), M. Furutani (Kumamoto University), K. Toyooka (RIKEN), M. Sato (RIKEN), Y. Kodama (Utsunomiya University), and H. Takeuchi (Nagoya University) for helpful discussions and to T. Uemura (Ochanomizu University) for providing "Deep" cells. *arg1-3* was a kind gift from P. Masson (University of Wisconsin–Madison). mRFP1-Spo20p-PABD was a kind gift from M. Potocký (Czech Academy of Sciences). The support of plant cultivation rooms was provided by the Model Plant Research Facility of the National Institute for Basic Biology. We also thank W. Takase, H. Motomura, K. Miyoshi, M. Hamada, Y. Yamada, and Y. Soma for technical assistance; the Salk Institute Genomic Analysis Laboratory for providing the sequence-indexed *Arabidopsis* transfer DNA (T-DNA) insertion mutants; and the *Arabidopsis* Biological Resource Center and GABI-Kat for providing seeds of the *A. thaliana* T-DNA insertion mutants and lipid biosensor lines (P5R and P24Y). **Funding:** This work was supported by Japan Society for the Promotion of Science (JSPS) KAKENHI, Grant-in-Aid for Scientific Research 19H03254 (M.T.M.); JSPS KAKENHI, Grant-in-Aid for Scientific Research on Innovative Areas 18H05488 (M.T.M.), 18H05491 (M.T.), and 18H05492 (T.H.); Japan Science and Technology Agency (JST), Core Research for Evolutionary Science and Technology (CREST) JPMJCR14M5 (M.T.M.); Takeda Science Foundation (M.T.M.); Naito Foundation (M.T.M.); JSPS KAKENHI, Grant-in-Aid for Scientific Research 22H00302 (H.Y.Y.); JSPS KAKENHI, Grant-in-Aid for Challenging Exploratory Research 20K21117 (H.Y.Y.); JSPS KAKENHI, Grant-in-Aid for Scientific Research 20H03289 (T.H.); JST, CREST JPMJCR2121 (T.H.); JSPS KAKENHI, Grant-in-Aid for Early-Career Scientist 18K14731 (M.N.); and JSPS KAKENHI, Grant-in-Aid for Early-Career Scientist 20K15826 (H.S.). **Author contributions:** Conceptualization: M.T.M., T.N., and H.S. Design of experiments: M.T.M., T.N., H.S., and M.T. Methodology: H.Y.Y. and M.T. Investigation: T.N., H.S., S.M., M.N., Y.A., T.H., Y.H., and T.H. Funding acquisition: M.T.M., M.N., M.T., T.H., H.Y.Y., and H.S. Project administration: M.T.M. Supervision: M.T.M. Writing: M.T.M., T.N., H.S., M.T., and T.H. **Competing interests:** The authors declare no competing financial interests. **Data and materials availability:** All materials are available upon request subject to a material transfer agreement. All data are available in the main text or the supplementary materials.

SUPPLEMENTARY MATERIALS

science.org/doi/10.1126/science.adh9978
Materials and Methods
Figs. S1 to S25
Table S1
References (*50*–*70*)
MDAR Reproducibility Checklist
Movies S1 to S9

Submitted 11 April 2023; accepted 2 August 2023
Published online 10 August 2023
10.1126/science.adh9978